Computer Assisted Methods in Engineering and Science
30(3): 277–290, 2023, doi: 10.24423/cames.631

This article belongs to the *Special Issue on Digital Twin Empowered Internet of Intelligent Things for Engineering Cyber-Physical Human Systems* edited by C. Venkatesan, Y.-D. Zhang, Q. Xin

A Novel Framework for Fetal Nuchal Translucency Abnormality Detection Using Hybrid Maxpool Matrix Histogram Analysis

Deepti VERMA[1)*], Shweta AGRAWAL[2)]

[1)] *Department of Computer Science and Engineering, SAGE University, Indore, Madhya Pradesh, India*

[2)] *Institute of Advance Computing, SAGE University, Indore, Madhya Pradesh, India; e-mail: shweta.sagecse@gmail.com*

[*] *Corresponding Author e-mail: deeptivv@rediffmail.com*

Birth defects affect 1 to 3 percent of the population and are mostly detected in pregnant women through double, triple, and quadruple testing. Ultrasonography helps to discover and define such anomalies in fetuses. Ultrasound pictures of nuchal translucency (NT) are routinely used to detect genetic disorders in fetuses. The NT area lacks identifiable local behaviors and detection algorithms are required to classify the fetal head. On the other hand, explicit identification of other body parts comes at a higher cost in terms of annotations, implementation, and analysis. In circumstances of ambiguous head placement or non-standard head-NT relationships, it may potentially cause cascading errors. In this research work, a linear contour size filter is used to decrease noise from the image, and then the picture is scaled. Then, a novel hybrid maxpool matrix histogram analysis (HMMHA) is proposed to enhance the initiation and progression. The training and assessment were conducted using a dataset of 33 ultrasound pictures. Extensive testing shows that the direct method reliably identifies and measures NT. The suggested model may assist doctors in making decisions about pregnancies with fetal growth restriction, particularly for patients who have nuchal translucency or congenital anomalies and do not require induced labor due to these abnormalities. The performance of the proposed technique is analyzed in terms of error rate, sensitivity, Matthews correlation coefficient (MCC), accuracy, precision, recall, and F1-score. The error rate of the proposed model is 28.21% and it is found to be better when compared with the conventional approaches. Finally, the error prediction is compared with the existing models obtained from the medical dataset of pregnant women to identify fetal abnormality positions.

Keywords: nuchal translucency, genetic disorders, hybrid maxpool matrix histogram analysis, pregnant women, machine learning.

1. Introduction

Down syndrome (DS), commonly known as trisomy 21, is a serious chromosomal disease that affects one out of every 700 newborn babies. Typically, each chromosome has two copies, but DS is a hereditary disorder in which chromosome 21 has three copies, all or part of a third copy is an extra one. It is a hereditary disorder caused by an extra 21st chromosome. Mild to severe developmental problems emerge from the disorder, affecting both cognitive capacity and physical growth. Individuals with DS typically have distinctive physical traits, health difficulties, and cognitive development that vary. DS may be identified before or after a baby is born via several screenings and tests. Certain morphological characteristics of DS fetuses differ from euploid fetuses, and for DS these characteristics are the facial fronto-maxillary (FMF) angle, the lack of a nasal bone, and greater nuchal translucency [1]. In the early trimester of pregnancy, trained operators use ultrasound images to assess the thickness of the NT. The manual screening method is time-consuming and prone to errors. As a result, it is critical to provide an accurate and automated NT measuring method. The thickness of an object is measured using the NT method; first, the area is measured and then the thickness is calculated. The dark and bright contrast may exist in several areas in the image, making automatic area recognition a difficult challenge. Both medical specialists and current identification algorithms depend on the location of several other bodily regions with distinct patterns [2]. For nuchal translucency detection an ultrasound scan is used. Figure 1 illustrates the fluid-filled zone under the fetus's neck skin, which sonographically appears as an anechogenic area (i.e., a black zone in grayscale pictures) between two echogenic areas (i.e., bright zones) [3]. The best time to test NT thickness is between the eleventh and twelfth weeks when the NT achieves its maximum thickness, and after that, it gradually goes away.

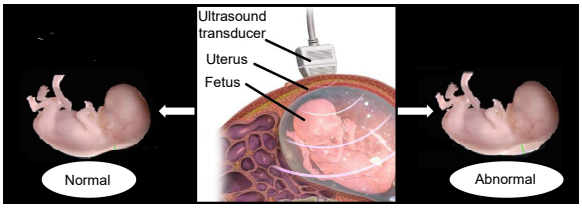

Fig. 1. Nuchal translucency detection by ultrasound scan.

The current work presents the following benefits: 1) easy-to-use internet and mobile applications that support a machine learning approach to predict fetal care; 2) data from pregnant women admitted to a diagnostics facility is used to teach the major techniques to determine fetal health based on patient's medical data and other information including family history. Following that, the pre-

ceding investigation is discussed, methods and technical information about the developed framework are provided, various aspects and weights in the data source are analyzed, results from volunteer patients are analyzed, and lastly, the study is brought to a conclusion. The main contribution of the paper is to detect the NT abnormality using hybrid maxpool matrix histogram analysis (HMMHA). The nuchal translucency test determines the thickness of the nuchal fold. This is the tissue at the back of a baby's neck in the womb. This thickness is used to determine the infant's likelihood of DS and other genetic abnormalities.

2. Related works

NT measurements and comprehensive follow-up information were retrieved from the project's prospective database for fetal down screening [4]. Due to pre-existing medical conditions, pregnancies with genetic or structural abnormalities were excluded from the study. The selected pregnancies were classified into the increased nuchal translucency (INT) (greater than 95th%) group and the normal (less than 95th%) group. In [5], The researchers examined the usefulness of chromosomal microarray analysis (CMA) and whole exome sequencing (WES) in fetuses with increased NT. A total of 374 singleton pregnancies with gestational ages ranging from 11 to $13 + 6$ weeks were studied. WES is a procedure carried out in a lab to identify the nucleotide sequence, particularly of the exonic portions of a person's genome and associated sequences, which make up about 1 percent of the whole DNA sequence.

In [6], convolutional neural learning techniques were studied and compared. Biometric characteristics extracted and measured via segmentation methods were used in neural network identification of fetal abnormalities. In [7], machine learning was used to create and evaluate an algorithm for maternal postpartum readmissions due to complications of hypertensive disorders of pregnancy. In [8], the authors' goal was to accurately predict fetal weight at different stages of pregnancy without an ultrasound screening. For obstetricians, machine learning can provide exact predictions, and pregnant women may benefit from an effective and efficient self-monitoring method in addition to normal treatment options. To support their findings, the authors used data from 4212 intrapartum observations.

A variety of AI-powered methods for predicting fetal stage categories were presented in [9]. Multi-layer architecture of a sub-adaptive neuro fuzzy inference system (MLA-ANFIS) architectures are implemented on a continuous cardiotocography (CTG) dataset using multiple input characteristics, neural networks (NN), deep stacked sparse auto-encoders (DSSAEs), and deep-ANFIS algorithms. In [10], prenatal analyzes of fetal anomalies in 10 414 fetuses and neonates were compared with all postnatal diagnoses of congenital abnormali-

ties between 2006 and 2013. For fetuses with increased NT (≥ 3.5 mm) who received standard prenatal testing, genome sequencing (GS) (>30-fold) was used in a retrospective study [11].

The goal of the research in [12] was to conduct a population-based, individual record linkage study to establish the best way to define an enlarged nuchal translucency for detecting atypical chromosomal abnormalities. In [13], the authors studied 52 400 pregnant patients who came in for a normal ultrasound scan between 35- and 36-weeks' gestation. All pregnancies had a previous scan at 18–24 weeks, and 47 214 also had a scan at 11–13 weeks. Pregnancies that were found in a normal delivery or death have been included, but those with congenital anomalies were eliminated. The nature and occurrence of such anomalies were established, and anomalies were categorized per the impacted main organ. The objective of [14] was to focus on the outcome and medical value of trio-based rapid WES in pregnancies of fetuses with a variety of congenital anomalies that were diagnosed by ultrasound scans.

In [15], 55 fetuses were studied to learn more about them. Two or more independent significant fetal malformations, hydrops fetalis, or a significant fetal abnormality and a first-degree relation with a similar condition have all been used as criteria for inclusion. To identify cardiac subsets and structural anomalies in fetal ultrasound recordings, the authors suggested a novel supervised object detection with normal data only (SONO) architecture focusing on a convolutional neural network (CNN) [16]. The detection probability was measured and described using a barcode-like chronology and an anomaly score for every frame was obtained. In [17], machine learning-based quick and accurate automatic testing played a vital role in assessing bone fragments on computed tomography (CT) scanning. Despite the requirement in drug safety assessment, animal fetus micro-CT scan study is uncommon due to the time-consuming data collection and interpretation.

3. Proposed methodology

The proposed methodology employs ensemble machine learning approaches to classify ultrasound pictures of fetal abnormality, as shown in Fig. 2. The overall strategy includes: a) ultrasound fetal images, b) preprocessing, and c) image augmentation, followed by augmentation output and performance analysis for validation.

3.1. Fetal image dataset

The fetal images were manually collected from Boston Children's Hospital. About 33 ultrasound fetal images were taken and analyzed for abnormalities.

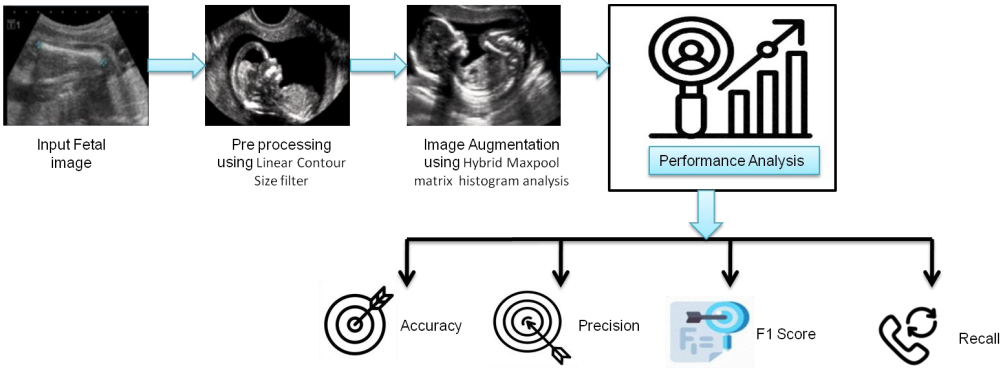

FIG. 2. The schematic of the proposed flow diagram.

3.2. Preprocessing

A linear contour size filter is an iterative technique for recovering the intensities in ultrasonic images. All picture and frame data were rescaled, and a clipped x and y rectangle comprising the majority of the field of view but omitting the vendor logo and ultrasonic control indications was created. Each picture was also normalized by removing the mean intensity value and dividing by the pixel standard deviation. Moreover, the linear contour size filter outperforms everything else. The linear contour size filter is a looping algorithm that simulates the diffusion process in the following way:

$$\frac{\rho N(a,b,t+1)}{\rho m} = \operatorname{div}(\nabla N), \tag{1}$$

where $N(a,b,t+1)$ can be written as:

$$N(a,b,t+1) = N(a,b,t) + \operatorname{div}(H(|\nabla N|)\nabla N), \tag{2}$$

where ρ denotes a noise filter, ∇N denotes the summation of noise scores, a, b, t are values of the neighboring pixels' noise, and m is the image's pixel count.

For two reasons, noisy pixels are filtered out much more rapidly than edge pixels. The first is that, according to the equation, gradients in opposing directions cancel each other out, but this is not the case with noise pixels. Second, the anisotropic diffusion filter has a significant influence only when a large number of neighbors have a big gradient magnitude. Noisy pixels are scattered around the image rather than concentrated in one spot, and therefore their intensity is distinct from the surrounding pixels,

$$M(a,b,K+1) = N(a,b,K) + \frac{\lambda}{\left|\delta_{(a,b)}\right|} \sum_{(j,i)\in\delta_{(a,b)}} H\left(\left|\nabla N_{(j,i)}^{(a,b)}\right|\right) \nabla N_{(j,i)}^{(a,b)}. \tag{3}$$

The pixel signature of edge pixels, on the other hand, is far more similar to that of the bulk of pixels in their proximity. This assists in the elimination of contaminants that may make subsequent morphological procedures more difficult to identify abnormalities:

$$\nabla e_{90^\circ}^{(a,b)} = N(a, b-1, K) - N(a, b, K), \tag{4}$$

$$\nabla e_{-90^\circ}^{(a,b)} = N(a, b+1, K) - N(a, b, K), \tag{5}$$

$$\nabla e_{0^\circ}^{(a,b)} = N(a+1, b, K) - N(a, b, K), \tag{6}$$

$$\nabla e_{180^\circ}^{(a,b)} = N(a-1, b, K) - N(a, b, K). \tag{7}$$

3.3. Image augmentation-based hybrid max pool matrix histogram

Color constancy is a vital stage in the hybrid maxpool matrix histogram, which is a common picture improvement approach. By taking a low-level approach to color constancy, a link between color constancy and an image's histogram is established. The picture is represented in the hybrid max pool matrix model

$$d_c = \int s(\lambda)\, l(\lambda)\, C_c(\lambda) d\lambda, \tag{8}$$

where λ is the visible light's wavelength, $s(\lambda)$ is the reflectivity of the surface, $l(\lambda)$ is the source of light, and $C_c(\lambda)$ is the camera sensitivity in the channel d.

Consider the light source's projected color on red, green, and blue (RGB) space, with the aim of color constancy. Assumptions have been made to reach this aim. As an example, consider the max-RGB, which uses the three channels' maximum responses to determine the light source's approximate location and intensity. In addition, the gray-world theory posits that the scene's average reflectance is achromatic. Recent developments have converged on the following:

$$\left(\frac{\int |f(x)|^\beta dx}{\int dx} \right)^{1/\beta} = Aa, \tag{9}$$

where x is the pixel's coordinate, A is an arbitrarily high number, β is a parameter, and $a = [a_r, a_g, a_b]^T$ is the normalized estimation of the light source.

The left-hand side of Eq. (9) may be expressed from the perspective of an image histogram:

$$\left(\frac{\int |f(x)|^{\beta} dx}{\int dx}\right)^{1/\beta} = \begin{pmatrix} \left(Q_r^T h_r^{\beta}\right)^{1/\beta} \\ \left(Q_g^T h_g^{\beta}\right)^{1/\beta} \\ \left(Q_b^T h_b^{\beta}\right)^{1/\beta} \end{pmatrix}, \tag{10}$$

where $h_n^{\beta} = [h_{n1}^{\beta}, ..., h_{nK}^{\beta}]^T$. The relationship between white balance and histogram is revealed, assuming a picture is provided, and determined as:

$$a_n(\beta) = \frac{\left(Q_r^T \widetilde{h}_r^{\beta}\right)^{1/\beta}}{\sqrt{\sum_{c=r,g,b} \left(Q_r^T \widetilde{h}_r^{\beta}\right)^{2/\beta}}}. \tag{11}$$

Thus, the hybrid maxpool matrix histogram ($\widetilde{h}_c$) is as follows:

$$\widetilde{h}_c = \frac{1}{e_c(\beta)\sqrt{3}} \widetilde{h}_c. \tag{12}$$

This is a linear process. The histogram-based hybrid max pool matrix algorithm's most notable characteristic is the transform linearity.

Algorithm 1 for Image Augmentation
if (there is no trained model available) **then**
load input
pixel to image conversion
image conversion to grayscale
grayscale picture histogram equalization
detect the edges from the images
resize all pixels' value
augment data by rotation, resizing, and zooming
train (70%), validation (15%), test (15%) ← dataset
save trained model
else
load trained model
test model with the test dataset
image splitt into normal and abnormal
error rate analyzed
IoU measured

4. Performance analysis

In this section, efficient techniques based on linear contour size filter and HMMHA are proposed and developed for NT image augmentation. The performance of the system is employed in the average pixel-level distance between the ground-truth point and the projected center point as an assessment criterion for center point identification. The NT area is defined as a rectangular rectangle with a 4:3 aspect ratio centered at the expected center point. To ensure that the rectangular area contains NT, then set the height to 128 pixels, which is almost twice the greatest NT region height. True positives are anticipated NT areas that include ground-truth center points, whereas false positives are predicted NT regions that do not contain ground-truth center points. The proposed work is compared to three existing networks: ultrasound networks (U-Net) [2], residual networks (ResNet-18) [18], and densely connected convolutional networks (DenseNet-121) [19].

Data augmentation improved performance significantly, as shown in Table 1. Compared to existing networks, the proposed model outperformed them, suggesting that it is well-suited to the task of NT augmentation. Figure 3 depicts the intersection over union (IoU) detection, with the green box indicating ground-truth bounding box and the orange box indicating that the predicted bounding box was 97% accurate.

Table 1. Comparative results for error rate and intersection over union (IoU) for the NT augmentation.

Algorithm	Error rate [%]	IoU
U-Net [2]	41.69	0.6991
ResNet-18 [18]	50.39	0.6686
DenseNet-121 [19]	50.21	0.6354
Hybrid maxpool matrix histogram (proposed)	28.21	0.9289

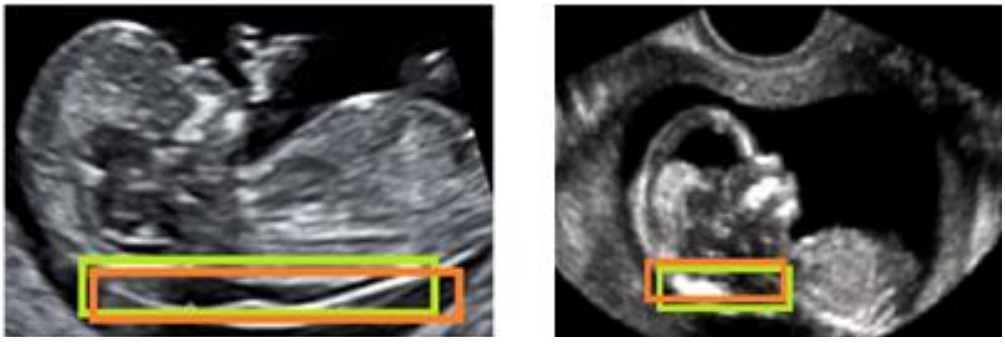

Fig. 3. NT augmentation visualization.

Figure 4 shows a percentage comparison of the error rate for the existing and proposed methods. Compared to the existing techniques, the proposed method has a low error rate.

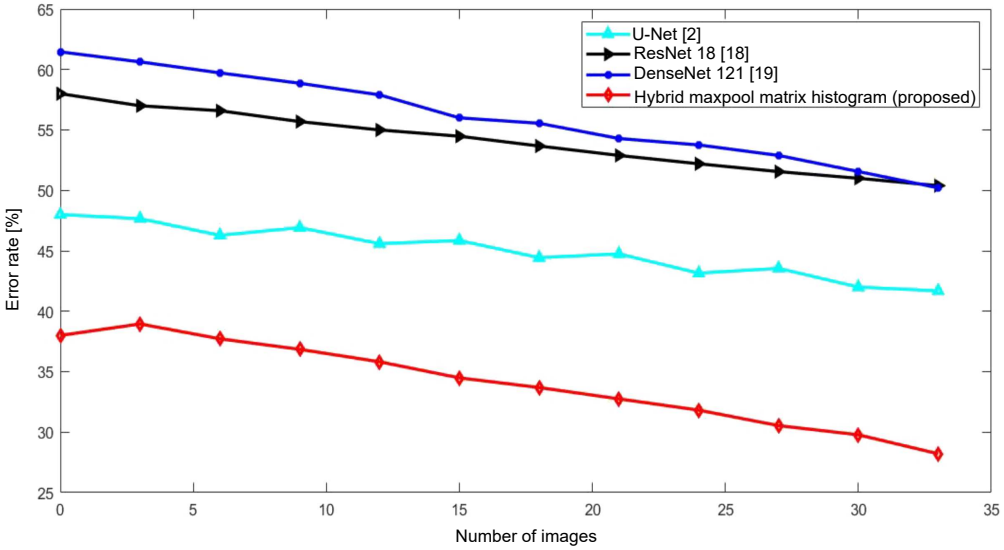

FIG. 4. Error rate vs. the number of images.

A total of 33 images were taken and used the suggested algorithm to divide them into two categories: normal and abnormal, as shown in Fig. 5. It is noticed

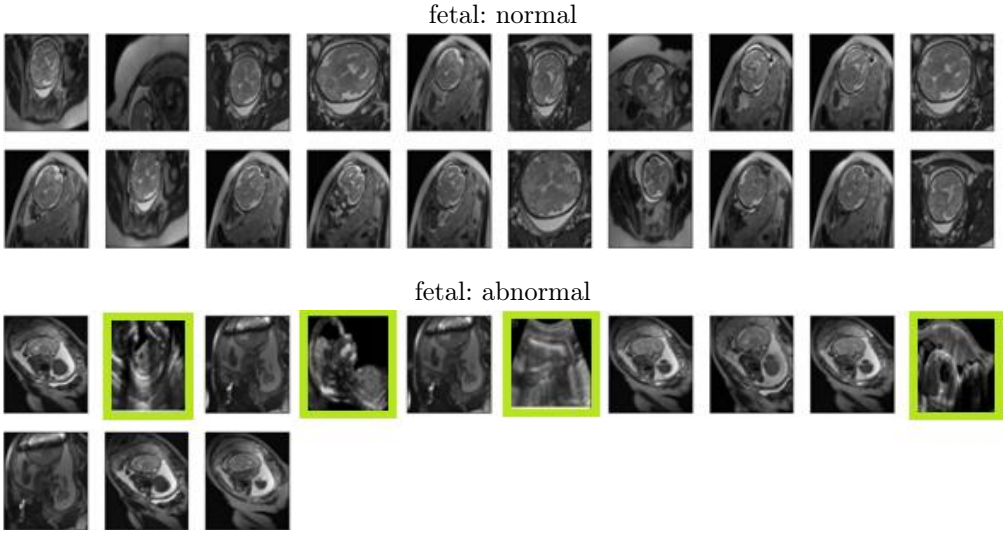

FIG. 5. Final result for the data augmentation.

that the photographs with the highest risk area (in the green box) indicate that the water content is low level (in mm), as shown in Fig. 5. The performance of the proposed technique is analyzed in terms of sensitivity, MCC, accuracy, precision, recall, and F1-score as follows.

4.1. Sensitivity

Consider a medical diagnostic test as an example. The test is capable of appropriately identifying patients who are suffering from the disease being tested for. The sensitivity of a test used to diagnose a condition (also known as the detection rate in a clinical context) is the proportion of persons who test positive for the disease among those who have it. Equation (13) may be used to represent this mathematically

$$\text{Sensitivity} = \frac{t_p}{t_p + f_n}. \tag{13}$$

When compared to the existing approaches, such as machine learning algorithm (MLA), feed forward neural network algorithm (FFNN), ultrasound imaging techniques (UIT), and adaptive risk prediction system (ARPS), the proposed method has higher sensitivity.

4.2. Matthews correlation coefficient (MCC)

The MCC is a contingency matrix technique for determining the Pearson product-moment correlation coefficient between actual and anticipated data. The following is a summary of MCC's entries

$$\text{MCC} = \frac{(t_p t_n - f_p f_n)}{\sqrt{(t_p + f_p)\,(t_p + f_n)\,(t_n + f_p)\,(t_n + f_n)}}. \tag{14}$$

When compared to each other, the proposed approach has the highest MCC compared to the existing models.

4.3. Accuracy

There is a formula for calculating the number of samples that can be effectively classified. It determines how close the results are to the predicted outcome. It is calculated by dividing the total number of real positives and true negatives by the total number of expected positives and negatives

$$\text{Accuracy} = \frac{t_p + t_n}{t_p + t_n + f_p + f_n}. \tag{15}$$

The proposed approach has a high accuracy of 95% and the existing models have lower accuracy values.

4.4. Precision

Precision is a metric that counts the number of favorable occurrences that were properly anticipated. A properly expected positive example is calculated as a proportion of all successfully projected positive instances. To put it another way, the true positive is obtained by dividing the total of true and positive numbers

$$\text{Precision} = \frac{t_p}{t_p + f_p}. \tag{16}$$

The precision of the proposed method is comparatively higher than the existing models.

4.5. Recall

By dividing the number of true positives by the total number of true positives and false negatives in a sample of data, the recall rate can be calculated

$$\text{Recall} = \frac{t_p}{t_p + f_n}. \tag{17}$$

Recall for the existing approaches is lower when compared to the proposed method.

4.6. F1-score

The F1-score is obtained as the harmonic mean of precision and recall during a certain period. It is a statistical metric for evaluating performance. As a result, both false positives and false negatives are factored into this score

$$\text{F1-score} = \frac{2 \times \text{precision} \times \text{recall}}{\text{precision} + \text{recall}}. \tag{18}$$

The F1-score of the proposed approach is comparatively high when compared with the traditional methods.

The sensitivity, MCC, accuracy, precision, recall and F1-score of various techniques are compared with the proposed HMMHA method, and the parameters are listed in Table 2. From the obtained results, it is evident that the proposed HMMHA performs better than the conventional approaches.

Table 2. Performance analysis of various algorithms with the proposed HMMHA method.

Methods	Sensitivity	Matthews correlation coefficient	Accuracy	Precision	Recall	F1-score
Machine learning algorithm (MLA)	74.8	64.5	73.8	68.4	65.5	68.9
Feed forward neural network algorithm (FFNN)	80.2	78.3	83.4	84.7	70.2	82.3
Ultrasound imaging techniques (UIT)	68.4	70.9	71.2	72.4	74.6	74.6
Adaptive risk prediction system (ARPS)	82.6	76.4	86.7	87.6	87.6	84.6
Proposed hybrid maxpool matrix histogram analysis (HMMHA)	90.4	92.6	95.8	98.1	97.2	96.3

5. Conclusion

In this research work, a machine learning-based NT detection and measurement method was described. The primary goal of this research was to create and apply a new system for identifying NT fetal abnormalities. In this work, several machine learning approaches, such as preprocessing and picture augmentation to assess abnormalities in the NT fetus, were used. According to qualitative and quantitative results, the whole system provides error rate and data augmentation NT detection findings in normal and abnormal conditions. The proposed model may support doctors in making decisions about pregnancies with fetal growth restriction, particularly for patients who have aberrant umbilical arterial flow or congenital anomalies and do not require induced labor due to these abnormalities. The performance of the proposed technique was analyzed in terms of error rate, sensitivity, MCC, accuracy, precision, recall, and F1-score. The error rate of the proposed model is 28.21% and it is found to be better compared with the other approaches.

References

1. P.S. Lakshmi, M. Geetha, N.R. Menon, V. Krishnan, P. Nedungadi, Automated screening for trisomy 21 by measuring nuchal translucency and frontomaxillary facial angle, *2018 International Conference on Advances in Computing, Communications, and Informatics (ICACCI)*, pp. 1738–1743, Bangalore, India, 2018, doi: 10.1109/ICACCI.2018.8554914.
2. T. Liu *et al.*, Direct detection and measurement of nuchal translucency with neural networks from ultrasound images, [in:] *Smart ultrasound imaging and perinatal, preterm and paediatric image analysis*, PIPPI SUSI 2019, Lecture Notes in Computer Science, Vol. 11798, pp. 20–28, Springer, Cham, 2019, doi: 10.1007/978-3-030-32875-7_3.

3. G. Sciortino, D. Tegolo, C. Valenti, Automatic detection and measurement of nuchal translucency, *Computers in Biology and Medicine*, **82**: 12–20, 2017, doi: 10.1016/j.compbiomed.2017.01.008.

4. S. Tiyatha, S. Sirilert, R. Sekararithi, T. Tongsong, Association between unexplained thickened nuchal translucency and adverse pregnancy outcomes, *Archives of Gynecology and Obstetrics*, **298**(1): 97–101, 2018, doi: 10.1007/s00404-018-4790-9.

5. S. Xue *et al.*, Genetic examination for fetuses with increased fetal nuchal translucency by genomic technology, *Cytogenetic and Genome Research*, **160**(2): 57–62, 2020, doi: 10.1159/000506095.

6. V. Rawat, A. Jain, V. Shrimali, S. Raghuvanshi, Performance analysis of different learning algorithms of feed forward neural network regarding fetal abnormality detection, [in:] Thanh Nguyen N., Kowalczyk R. [Eds], *Transactions on Computational Collective Intelligence XXX. Lecture Notes in Computer Science*, Vol. 11120, pp. 118–132, Springer, Cham, 2018, doi: 10.1007/978-3-319-99810-7_6.

7. M.K. Hoffman, N. Ma, A. Roberts, A machine learning algorithm for predicting maternal readmission for hypertensive disorders of pregnancy, *American Journal of Obstetrics & Gynecology MFM*, **3**(1): 100250, 2021, doi: 10.1016/j.ajogmf.2020.100250.

8. Y. Lu, X. Fu, F. Chen, K.K. Wong, Prediction of fetal weight at varying gestational age in the absence of ultrasound examination using ensemble learning, *Artificial Intelligence in Medicine*, **102**: 101748, 2020, doi: 10.1016/j.artmed.2019.101748.

9. M.S. Iraji, Prediction of fetal state from the cardiotocogram recordings using neural network models, *Artificial Intelligence in Medicine*, **96**: 33–44, 2019, doi: 10.1016/j.artmed.2019.03.005.

10. C. Rydberg, K. Tunón, Detection of fetal abnormalities by second-trimester ultrasound screening in a non-selected population, *Acta Obstetricia et Gynecologica Scandinavica*, **96**(2): 176–182, 2017, doi: 10.1111/aogs.13037.

11. K.W. Choy *et al.*, Prenatal diagnosis of fetuses with increased nuchal translucency by genome sequencing analysis, *Frontiers in Genetics*, **10**: 761, 2019, doi: 10.3389/fgene.2019.00761.

12. L. Hui *et al.*, Reexamining the optimal nuchal translucency cutoff for diagnostic testing in the cell-free DNA and microarray era: Results from the Victorian Perinatal Record Linkage study, *American Journal of Obstetrics and Gynecology*, **225**(5): 527.e1–527.e12, 2021, doi: 10.1016/j.ajog.2021.03.050.

13. A. Ficara, A. Syngelaki, A. Hammami, R. Akolekar, K.H. Nicolaides, Value of routine ultrasound examination at 35–37 weeks' gestation in diagnosis of fetal abnormalities, *Ultrasound in Obstetrics & Gynecology*, **55**(1): 75–80, 2020, doi: 10.1002/uog.20857.

14. C. Deden *et al.*, Rapid whole exome sequencing in pregnancies to identify the underlying genetic cause in fetuses with congenital anomalies detected by ultrasound imaging, *Prenatal Diagnosis*, **40**(8): 972–983, 2020, doi: 10.1002/pd.5717.

15. N. Corsten-Janssen *et al.*, A prospective study on rapid exome sequencing as a diagnostic test for multiple congenital anomalies on fetal ultrasound, *Prenatal Diagnosis*, **40**(10): 1300–1309, 2020, doi: 10.1002/pd.5781.

16. M. Komatsu *et al.*, Detection of cardiac structural abnormalities in fetal ultrasound videos using deep learning, *Applied Sciences*, **11**(1): 371, 2021, doi: 10.3390/app11010371.

17. A. Fukuda, C. Han, K. Hakamada, Effort-free automated skeletal abnormality detection of rat fetuses on whole-body micro-CT scans, [in:] *2021 IEEE International Conference on Image Processing (ICIP)*, Anchorage, AK, USA, pp. 279–283, 2021, doi: 10.1109/ICIP42928.2021.9506216.

18. K. He, X. Zhang, S. Ren, J. Sun, Identity mappings in deep residual networks, [in:] B. Leibe, J. Matas, N. Sebe, M. Welling [Eds], *Computer Vision – ECCV 2016*, Lecture Notes in Computer Science, Vol. 9908, pp. 630–645, Springer, Cham, 2016, doi: 10.1007/978-3-319-46493-0_38.

19. G. Huang, Z. Liu, L. van der Maaten, K.Q. Weinberger, Densely connected convolutional networks, [in:] *2017 IEEE Conference on Computer Vision and Pattern Recognition (CVPR)*, pp. 4700—4708, Honolulu, HI, USA, 2017, doi: 10.1109/CVPR.2017.243.

Received May 30, 2022; revised version July 31, 2022;
accepted January 11, 2023.